Supplementary file

A full list of the major parts and items used for the customization of Parnon printer is provided in the Appendix. The Arduino code is available upon request.

i. Preparation of 3D printed structures for C. elegans experiments

After printing, the 3D parts are removed from the plotting medium and are placed on an unseeded NGM plate. If they are to be used immediately, i.e. in the next 24 hours, they are rinsed five times with deionized water, then are left to dry off excess moisture, in sterile conditions. If they are to be used in longer than 24 hours, then they are washed with 5% sodium hypochlorite, for 15 min on an orbital shaker, followed by five rinses with deionized water, 10 min on the orbital shaker, each. This precaution is necessary since the parts are not printed in sterile environment. Next, the plates are left to dry off excess moisture in sterile conditions. The plates can be sealed with parafilm and stored in 4°C for several days, in which case they need to reach room temperature before use. If the plates are used after a few weeks, some evidence of crystallization might be noticeable in the plate NGM (see for example **Figure 3**), but the overall suitability is not compromised.

ii. Actuation pressure

The linear actuator (**Figure 2** left panel Part Ci) is a NEMA-8 captive with a $1{:}\,1$ step stroke of $3\ \mu m$. We use a $1{:}\,4$ step ratio for an effective step stroke (l_{st}) of $0.75\ \mu m$. The actuator has a $38\ mm$ total stroke length and a volume capacity of $2{,}470\ mm^3$. A typical part design will utilize a volume of $50\ mm^3$. Parnon's capacity is roughly $50x$ the average print volume. It is powered by a 40V power supply through a TB6600 Stepper Motor Driver. The motor driver has

microstepping capability, a $1:2$ step stroke is then $1.5\ \mu m$. The linear actuator is rated for to run at $0.49\ A$, the motor driver is set to $0.5\ A$. This linear actuator was chosen because it has the highest stroke precision the manufacturer could offer. An early version of Parnon utilized a NEMA-14 linear actuator that had a lower stroke precision. A higher stroke precision results in higher quality prints. The parts in **Figures 2** right panel C, D, F, and **Figure 3** are printed with the early version of Parnon, wearing NEMA-14; the parts in **Figures 2** right panel A, B, E, **Figure 3**, and **Figure 5** are printed with the recent version of Parnon, featuring NEMA-8.

The Arduino card communicates with the motor driver by sending $5\ V$ pulses in a square wave. A user defined delay time (t_d) is how long the pulse is sustained for. Each pulse equates to one step taken by the linear actuator. A total print time (t_{pr}) is derived during the gCode writing process. The total number of steps, or pulses, during a print control the extruded volume of NGM. A theoretical extruded volume $(V_{ex.})$ can then be calculated.

$$Eq.1: \quad V_{ex} = \frac{l_{st} t_{pr}}{2 t_d}$$

By varying t_d, V_{ex} can be controlled. A lower t_d will result in a more fluent stepping process in the actuator and higher V_{pr}.

The gCode defines the layer height (h_l) and the print path length (l_{pr}). Using the nozzle ID (w_i), a theoretical print volume (V_{pr}) can be calculated.

$$Eq.2: \quad V_{pr} = h_i l_{pr} w_i$$

We refer to the designed ratio of the print as the ratio of V_{ex} to V_{pr}. Despite the Parnon's several features meant to limit the amount of liquid spreading, some amount of liquid spreading still occurs. A print quality comparison between prints that resulted while the liquid spreading

mitigations were active *vs* when the plotting medium and cooling effect were not used is presented in **Figure S4**.

The amount of liquid spreading the fully functioning Parnon experiences was studied so the actual width of a line of printed NGM becomes predictable and designable. Results of the line width experiment are shown in **Figure S1**. Four $20\ mm$ long lines of NGM were printed, with $5\ mm$ transitions. Two experiments, accelerating and decelerating, were repeated 3 times each. A relationship between the designed ratio (V_{ex}/V_{pr}) and the actual ratio (w_l/w_i) of the line width (w_l) to the nozzle ID (w_i). A designed ratio of ~0.9 equates to an actual ratio of 1.0.

We control the designed ratio by varying t_d in $Eq.1$, as the variables in $Eq.2$ are set by hardware and the previously written gCode and thus more difficult to vary. By setting $V_{ex}/V_{pr} = 0.9$ we expect $w_l/w_i = 1$, or the final line width after liquid spreading will be equal to the inner diameter of the nozzle.

iii. NGM compressive viscoelastic response

NGM in the 9.11mm ID syringe used in the latest version of the Parnon was tested at strain rates starting at $\dot{\varepsilon} = 0.2$, incrementing by 0.2 five times ending at $\dot{\varepsilon} = 1.0$ (**Figure 2** left panel Part A). $\sigma_{eq.}$ ranged from ~0.25 g/cm^2 at $\dot{\varepsilon} = 0.2$ to ~1.5 g/cm^2 at $\dot{\varepsilon} = 1.0$. Strain rates decrease inversely as the fill level in the syringe increases for a constant actuation speed [**Figure S5**]. In the 9.11mm ID syringe $t_{eq.} = \sim 300\ ms$.

NGM in the 12 mm ID syringe used in the early versions of the Parnon was tested 4 times. We found that $t_{eq.} \cong$ 600ms at a $\dot{\varepsilon} = 1.1$. (**Figure 2** left panel Part Bi). In the 12mm ID syringe $t_{eq.} =$ ~600ms. We believe the larger ID of this syringe caused the higher $t_{eq.}$ and $\sigma_{eq.}$ when compared to the lower syringe ID (9.11mm) in the current version of the Parnon.

It was found that $t_{eq.} = t_r$. The stress in the NGM during extrusion will increase with both the syringe ID and the strain rate ($\dot{\varepsilon}$). The time it takes to reach the inflection point increases with the syringe ID but is effectively constant across multiple strain rates. In practice, we found that $t_{eq.}$= 700ms with the 9.11mm ID syringe results in the most accurate extrusion timing.

The time t_{eq} it takes for the compressive stress σ_{eq} in the NGM to reach a high enough level to begin pushing a relatively viscous liquid through a nozzle with a small ID ($254\ \mu m\ -\ 400\ \mu m$) increases with strain rate. As part of the work done on optimizing Parnon there is a feature written in the code that automatically uses t_{eq} to build up to σ_{eq} immediately before beginning extrusion during a print. With this addition the Parnon begins extruding NGM at the right time. Before, the NGM often extruded late as time had to pass for σ_{eq} to be reached. We speculate that the NGM near the nozzle where the resulting curves rose above σ_{eq} before approaching it ($\dot{\varepsilon} = 0.4,\ 0.6.\ 0.8$) were more viscous and therefore required more stress to be extruded. In addition, σ_{eq} for $\dot{\varepsilon} = 0.6,\ 0.8$ are relatively close in value. We believe this occurs because of differing viscosity conditions in the NGM during extrusion.

iv. gCode and software communication

Modifying the hardware of an existing 3D printer compromised the communication the printer had with the original print head. To resolve this issue, we introduced a limit switch, an Arduino card, and a stepper motor driver.

Before every print, a few lines of gCode instruct the Parnon print head to hit the limit switch, thus signifying to the software that the print has begun.

An Arduino Uno board connected to a Stepper Motor Driver which in turn is connected to the linear actuator. A custom Microsoft Excel program that processes raw cartesian coordinates and head speed values outputs three essential printer inputs:

a) A gCode file that the DOBOT MOOZ-2 will interpret into XYZ axis actuation commands. The gCode file is loaded on a USB external drive or a micro SD card and placed in the appropriate slot on the Parnon.

b) The time between the custom print head hitting the limit switch and beginning actuation pressure. We refer to this value as delay one ($delay1$) and it is measured in milliseconds.

c) An array of step delays (measured in milliseconds), steps to take and the relative volume (Designed Ratio). The step delay (t_d) and number of steps (n) which correspond to a designed ratio of ~0.90 are inputted through the Arduino serial port.

Outlining the part is currently done in a custom Microsoft Excel program. Each coordinate XYZ that the print head will travel to during the print is individually assigned to a row in order. Upon executing the custom Microsoft Visual Basic program, the coordinates are processes and written into a gCode file. The gCode is processed by the existing firmware from DOBOT.

Time needs to pass between the print head hitting the limit switch and the point at which extrusion should begin. This time is referred to as delay one ($delay1$), and depending on the part design varies around $2.4\ s$. The viscoelastic response NGM has to compressive stress requires a significant amount of time ($t_{eq.} = 700\ ms$) to pass before sufficient stress has been reached for extrusion to commence. $t_{eq.}$ is included in $delay1$ and is referred to as $strain$ in the Arduino Code. Section iv of Supplementary file refers in detail to NGM's response to compressive stress.

The total print time (t_{pr}) is derived in the Excel program as a result of dividing the path length (l_{pr}) by the head speed (v_h). l_{pr} and v_h are defined in the gCode. Depending on the delay

time between each step (t_d), the number of steps for the actuator to take (n) so it stops extruding when the print stops can be calculated.

$$Eq.3: \quad n = \frac{t_{pr}}{2t_d}$$

Depending on the distance each actuator step is (l_{st}), discussed in more detail in the next section, there will be a specific calculatable volume for each selection of t_d. Multiplying the cross-sectional are of the syringe ($A_s = 65\ mm^2$) by the distance the actuator will travel during the print allows the theoretical total extruded volume (V_{ex}) to be calculated.

$$Eq.4: \ V_{ex} = A_s n l_{st}$$

Comparing this theoretical volume to the total print volume (V_{pr}) gives us what we refer to as the designed ratio (V_{ex}/V_{pr}). How this value compares to what can actually be observed and is discussed in detail in the next section.

v. Plotting medium

A COMSOL Multiphysics simulation was ran on $20\ mL$ of plotting medium in a $60\ mm$ diameter cylinder **(Figure 2** left panel Part C). A negative heat flux was placed on the bottom of the geometry to model the cooling effect of the Peltier device. The relationship between the heat flux ($Q,\ mW/cm^2$) and the temperature drop across the plotting medium ($\Delta T,\ ℃$) is described by $Eq.5$.

$$Eq.5: \quad Q = 90.91\Delta T$$

It was determined experimentally that after ~20min, $\Delta T = \sim 2.0$ ℃ (**Figure 2** left panel Part D). As a result of the COMSOL modeled relationship shown in $Eq.5$, $Q = 182\ mW/cm^2$. Over the whole area of the plotting medium ($2.83\ cm^2$) the energy exiting the plotting medium is $5.15\ W$. The Peltier device is rated at $6\ W$. The Parnon's cooling system operates at 86% efficiency. During a print, the NGM is being extruded into plotting medium that is ~13 ℃ less than the fastest

solidification temperature. A dynamic heat transfer model of NGM cooling in the plotting medium was not developed. NGM is extruded at ~65 ℃, however, ~29 ℃ above the fastest solidification temperature. Assuming that the thermal conductivities of NGM and the plotting medium are equal, then NGM would solidify the fastest if the plotting medium was also ~29 ℃ less than the fastest solidification temperature. There is another factor to consider, however, FDM relies on the previous layer remaining liquidous until the next layer is able to fuse. If the NGM solidifies too quickly the layers will not fuse together resulting in failed prints. While not quantified, we speculate that the limited ability of the Parnon's substrate cooling system is beneficial to the overall printing capability.

Supplementary figures

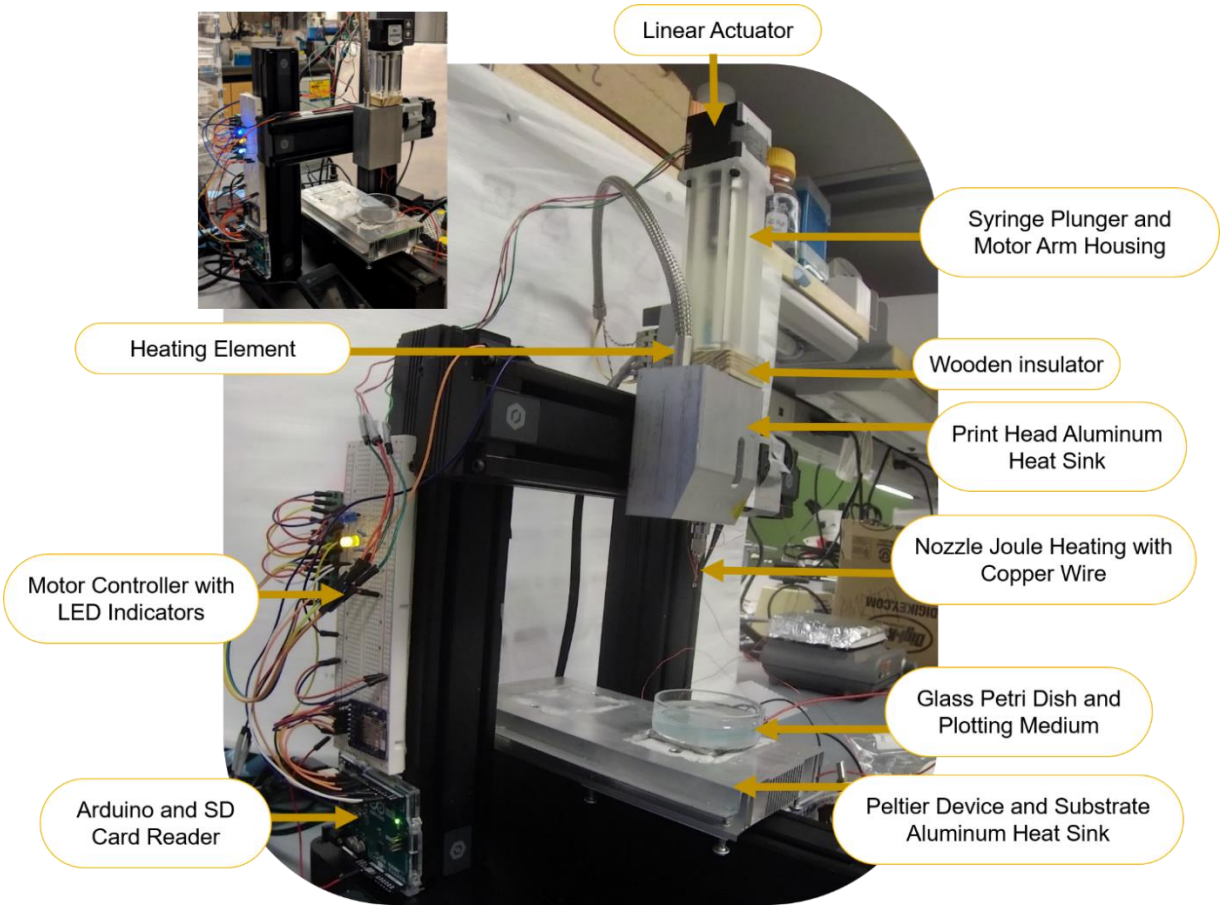

Figure S1. Overview of the Parnon printer. The major customized and house-made parts are indicated. Small inset: early version of the Parnon printer, in which a shorter linear actuator and syringe housing are featured.

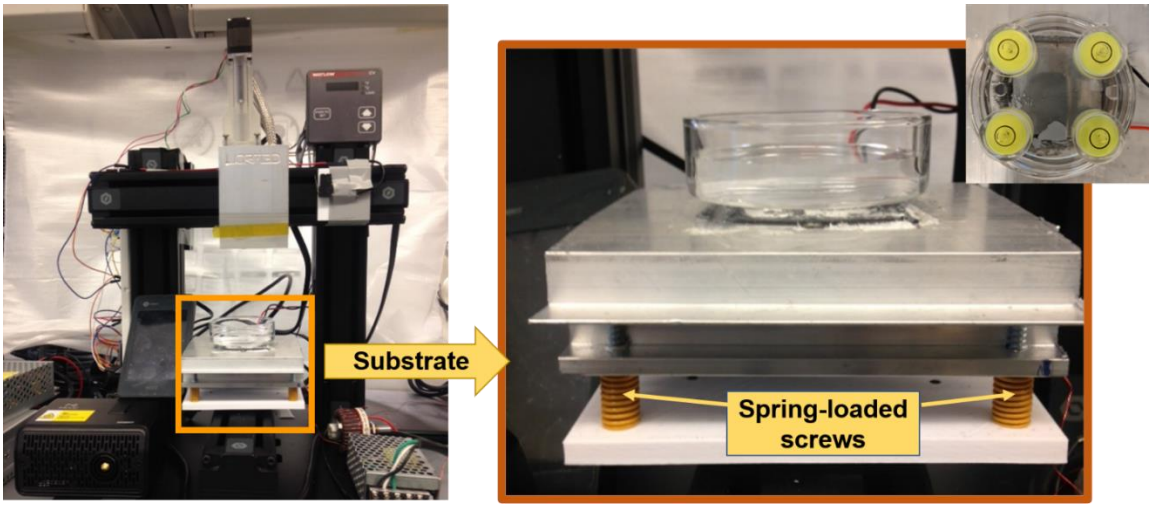

Figure S2. Four-point bed leveling system. Each corner of the substrate is equipped with a spring-loaded screw, to either raise or lower the corresponding corner of the substrate. Circular levels are placed at each corner of the substrate (small inset) and the screws are adjusted until each level reading matches the rest.

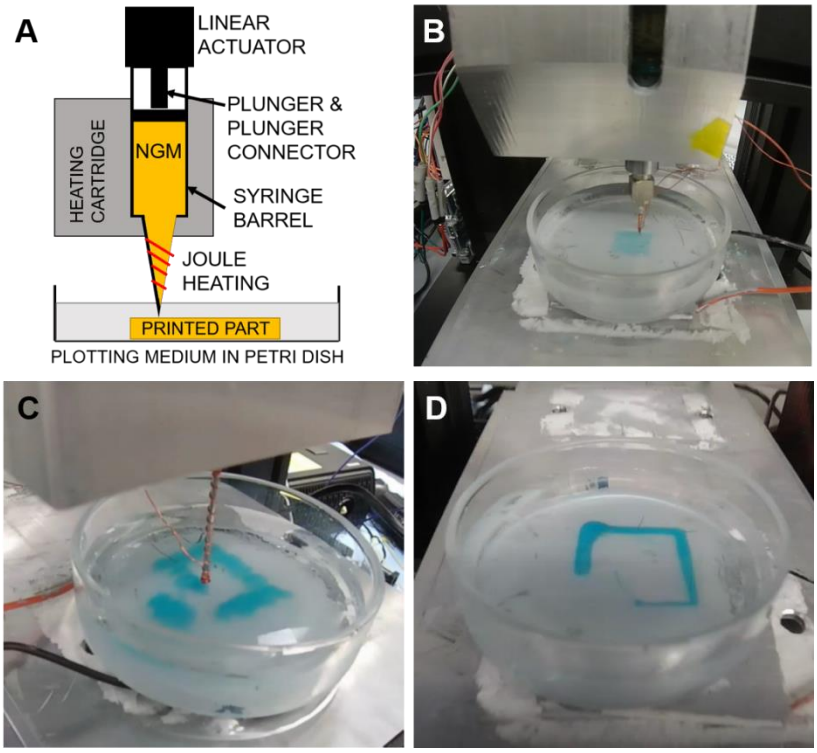

Figure S3. The printing apparatus and the nozzle joule heating detail. (**A**) Schematic of the syringe barrel containing liquid NGM, sitting inside the heating sink which contains the heating cartridge. The joule heating is illustrated around the protruding nozzle. (**B**) Printing a two-layer pad, as shown in Suppl. Fig. S3 A&B. (**C**) Printing a square structure; note the wider nozzle which results in thicker printed lines, compared to (D). A longer nozzle is used for demonstration

purposes. (**D**) A semi-finished square, still in the plotting medium; note the thinner lines compared to (C), as a result of the narrower nozzle used.

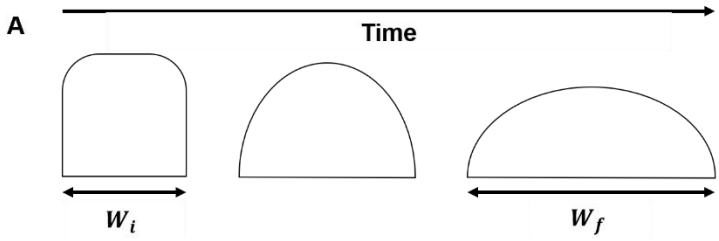

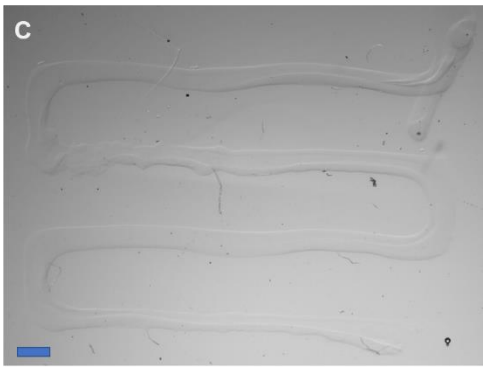

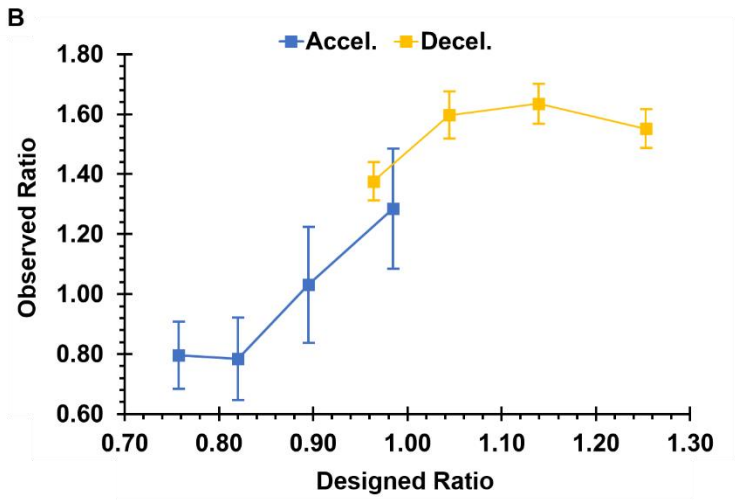

Head Speed	Designed Ratio	Observed Ratio	
		Mean	Std. Err.
Acceleration			
10	0.76	0.8	0.11
11	0.82	0.78	0.14
12	0.9	1.03	0.19
13	0.98	1.29	0.2
Deceleration			
13	0.96	1.38	0.06
12	1.04	1.60	0.08
11	1.14	1.63	0.07
10	1.25	1.55	0.06

Figure S4. Liquid spreading control and line width experiments. (**A**) Schematic of the cross section of a printed line that exhibits liquid spreading, evolving over time. The initial width (W_i) is the line width immediately after the line is extruded, which is approximately equal to the width of the nozzle. As time passes, the width of the line increases while the height decreases. The final width (W_f) is the line width after the equilibrium shape has been reached. (**B**) Graph showing the relationship between the ratios of designed line widths and observed line widths to W_i. A designed ratio of 1 means the expected value for W_f is equal to the width of the nozzle. The designed line width is the expected value for W_f based on user defined extrusion volume. An observed ratio of 1 means the final width (W_f) is equal to the width of the nozzle. The observed line width is the measured value for W_f after printing. Means with standard error bars are shown. To achieve an observed ratio of 1 (W_f = nozzle width) the design ratio needs to be ~0.90. Table shows data from line width experiments. (**C**) Image from the line width experiments. Four consecutive 20 mm long lines were printed with a head speed ranging from 10 mm/s to 13 mm/s. In four experiments, the head speed started at 10 mm/s and incremented 1 mm/s per line with an actuation speed of 13.4 $\mu m/s$. In another four experiments, the head speed started at 13 mm/s and decremented 1 mm/s per line with an actuation speed of 17.0 $\mu m/s$. The software that accompanies the

microscope used to take these pictures allows for measurements in pixels and subsequent conversion to mm. Scale bar: 2mm.

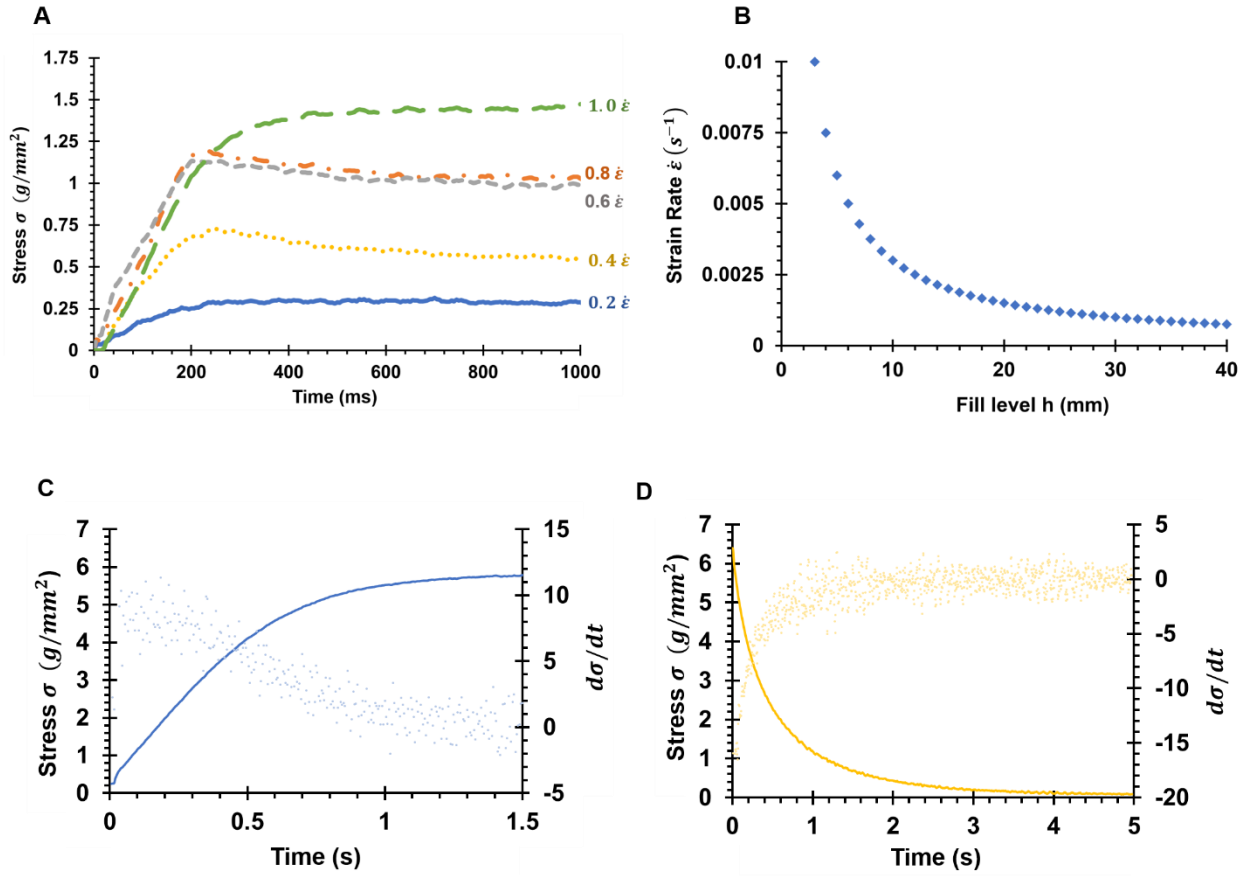

Figure S5. The viscoelasticity of NGM. The compressive strain rate is directly proportional to the equilibrium stress in the liquid NGM during extrusion.
(**A**) Graph showing how stress σ changes over time, for 5 different strain rates $\dot{\varepsilon}\ (s^{-1})$. NGM extruded at a constant actuation speed will result in increasing strain rates (see also Supplementary Fig. S5). (**B**) Strain rate varies with the NGM fill level in the syringe and the actuation speed. Study done with 30 $\mu m/s$ actuation speed. The syringe used in the Parnon is considered full at 50 linear millimeters of NGM. Eq. SF4 describes the inverse relationship of strain rate $(\dot{\varepsilon})$ to fill level (h) given a constant actuation speed (v). $Eq.\ SF4$: $\dot{\varepsilon} = \frac{h}{v}$. The values for strain rate (ε̇) are unique to the syringe used in the Parnon, but the trend is expected to apply in all cases of actuation pressure extrusion. (**C**): Comparison of increasing σ (continuous line, left y axis) and $d\sigma/dt$ (scatter plot, right y axis) over time (stress build up). When $d\sigma/dt$ reaches 0, the inflection point has been

reached. The time it takes for the inflection point to be reached is $t_{eq.}$. (**D**): Comparison of decreasing σ (continuous line, left y axis) and $d\sigma/dt$ (scatter plot, right y axis) over time (stress relaxation). When $d\sigma/dt$ reaches 0, the inflection point has been reached. The time it takes for the inflection point to be reached is t_r. It was found that $t_{eq.} = t_r = \sim 600\ ms$ at $\dot{\varepsilon} = 1.1$. Panels C and D: Compressive results using a 5mL, 12mm ID syringe and a 404 ID nozzle.

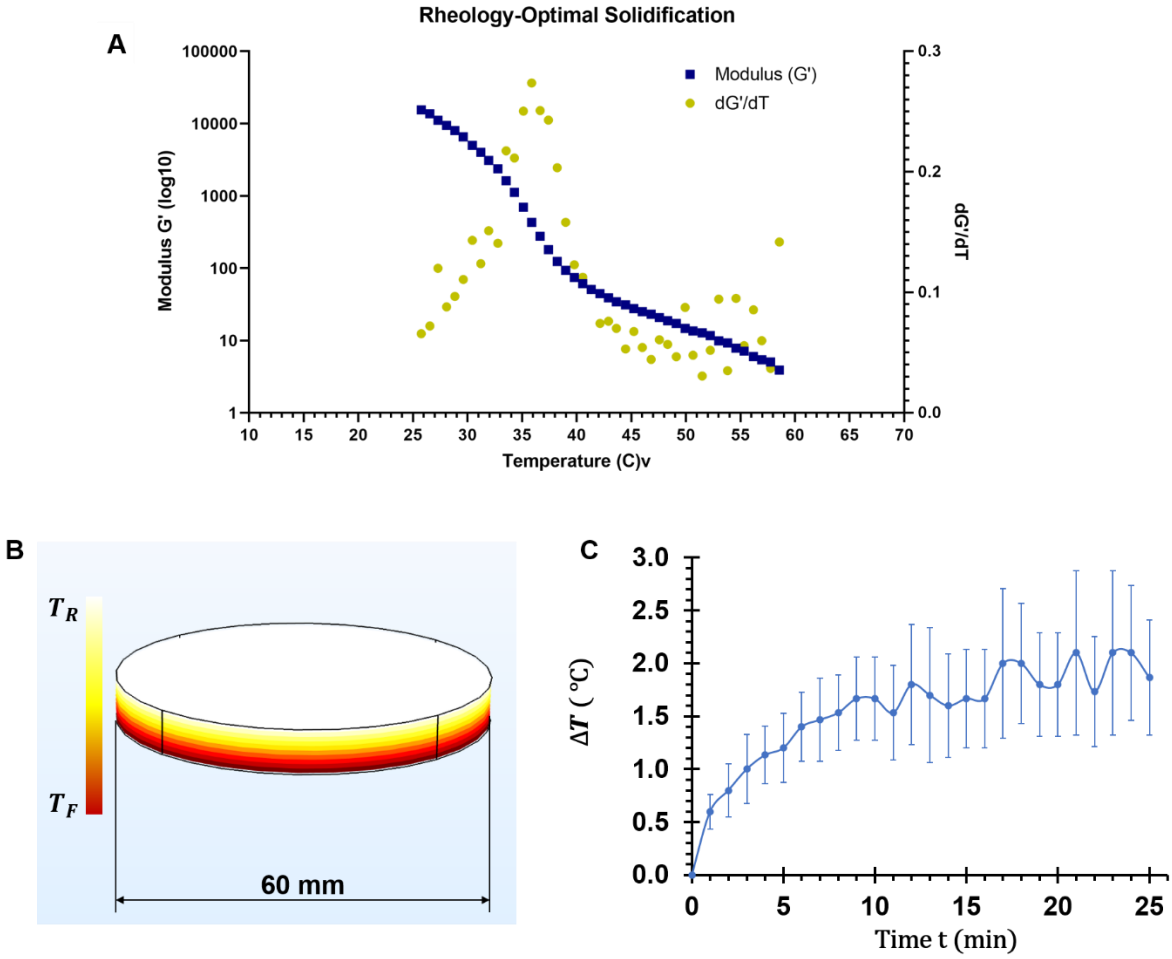

Figure S6. NGM solidification rheology, and heat flux model of the substrate. (**A**) Graph shows the storage modulus G' (blue squares, left y axis) and rate of change dG'/dT (green circles, right y axis) as a function of temperature. The highest value of dG'/dT corresponds to 35.9 ℃, meaning that at this temperature solidification occurs the fastest. Rheology experiment performed on a TA DHR2 Rheometer at a cooling rate of 5 ℃/min and an angular frequency of 1 rad/s. (**B**) COMSOL visualization of the temperature gradient across the plotting medium (plotting medium cylinder volume: 20 mL). The cooling source is the heat flux (Q) provided by the Peltier device beneath the substrate. The temperature drop (ΔT) is defined as $\Delta T = T_R - T_F$, where $T_R = 25$ ℃ (estimated room temperature) and T_F is dependent on the effective heat flux (Q). (**C**) Actual temperature drop over time, with mean of three independent experiments and standard error bars. The cooling levels out at a ΔT of ~2.0 ℃. Using Eq. F9 our Peltier device is achieving an effective heat flux of $182\ mW/cm^2$ or $\sim 5.15\ W$ over the entire 60 mm petri dish. Eq. F9 describes the linear relationship between Temperature Reduction (ΔT, in ℃) and Heat Flux (Q, in (mW/cm^2). *Eq. F9: ΔT=0.011Q*

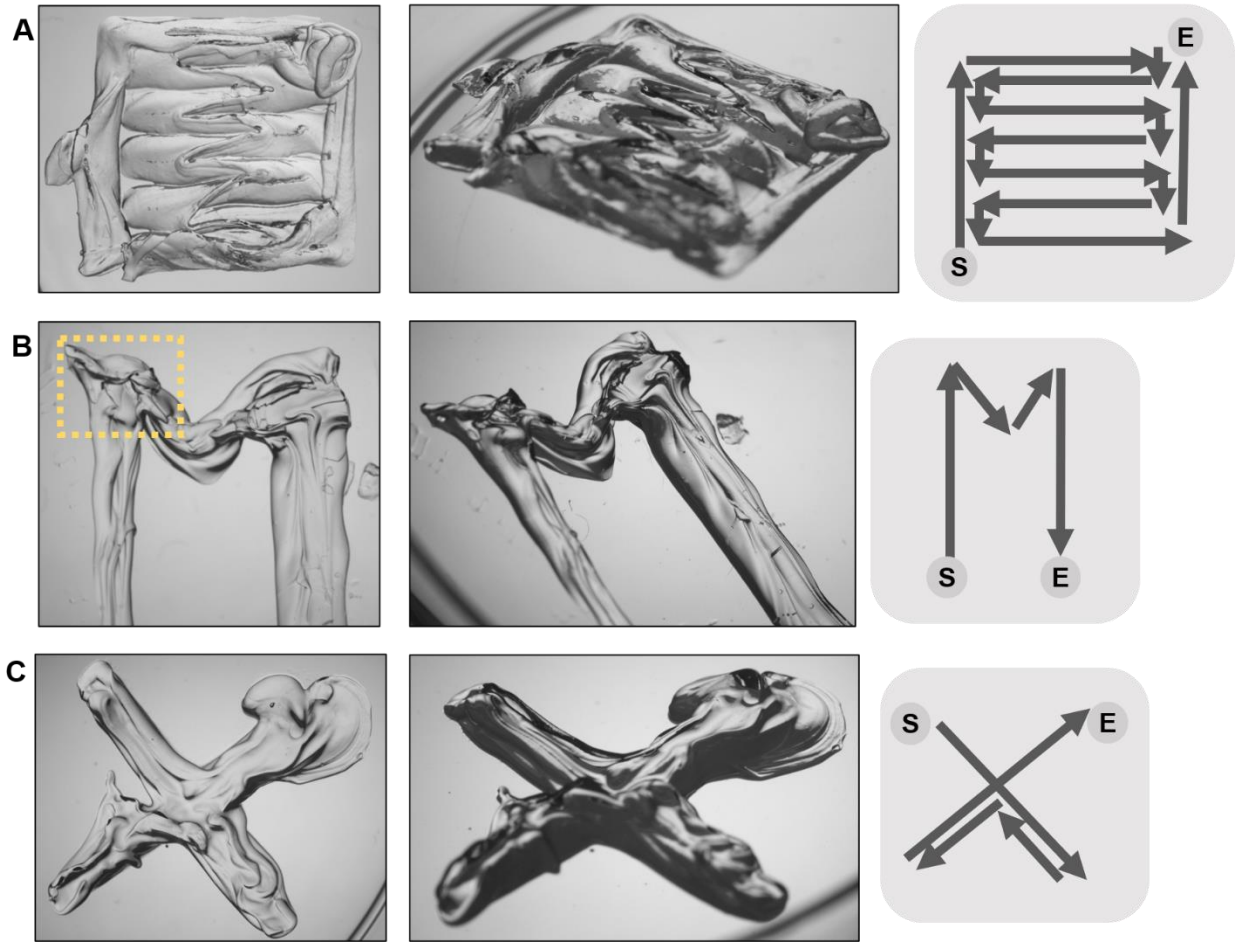

Figure S7. Parnon-printed structures and printing paths. These structures were printed with a larger diameter nozzle (400 μm – 1 mm ID) than the structures in Fig 5. (A) NGM pad, printed to test Parnon's ability to create continuous sheets. (B) M-shaped print, to test Parnon's ability to lay NGM lines in acute (<90°) angles, yellow frame indicates reduced printing quality area. (C) A cross-shaped print, to test Parnon's ability to print cross-shaped designs, without having to pause extrusion, relocate, and restart extrusion. All panels: Left: top view; middle: perspective view; right: schematic of printing path; S: start, E: end.

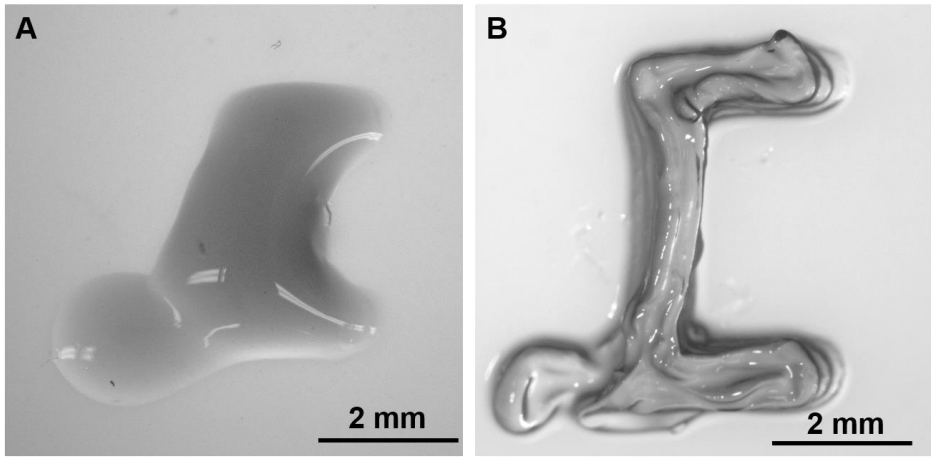

Figure S8. Printed part quality comparison with respect to plotting medium usage. (**A**) C-shaped part printed without plotting medium, exhibiting extensive liquid spreading, top view. (**B**) Same C-shaped design printed using plotting medium, with minimal liquid spreading, top view. This is the same C-shaped part as in Figure 5A & 5B.

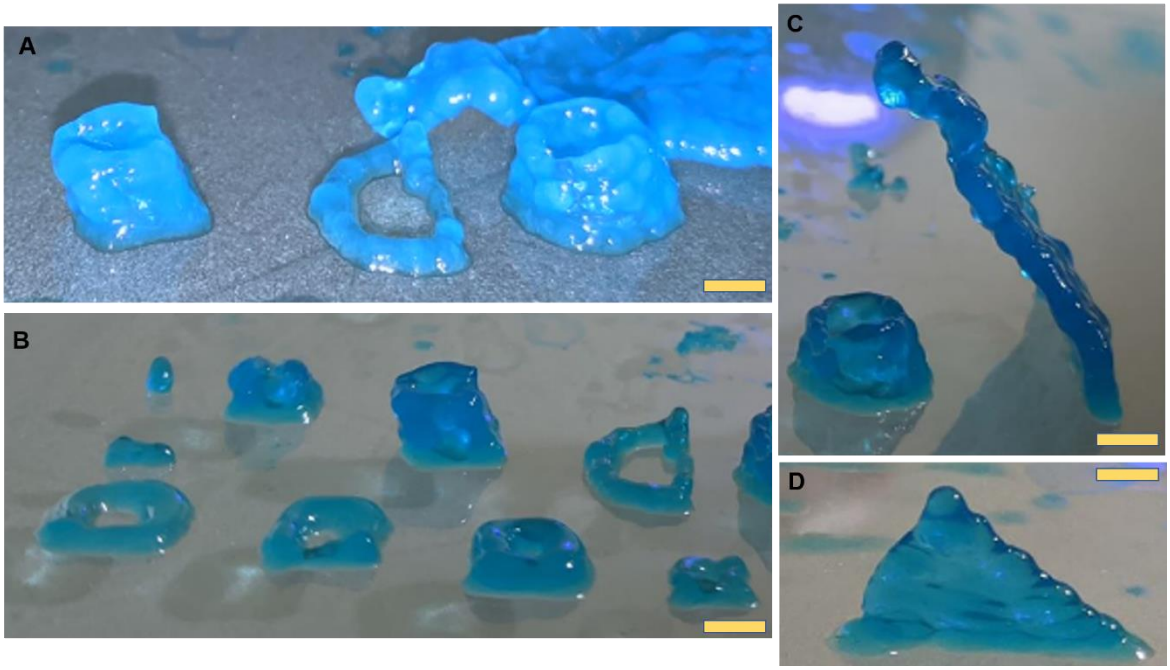

Figure S9. Printing attempts for multi-layer NGM parts. (**A**) Examples of 1- to 4-layer cylindrical structures, scale bar: 5mm. (**B**) Examples of 1- to 5-layer cylindrical structures, front row printed in the absence of plotting medium, scale bar: 6mm. (**C**) A 5-layer cylinder and a 14-layer triangular tilted wall (side view), scale bar: 6mm. (**D**) A12-layer triangular wall similar with the one in C, tilted forward (front view), scale bar: 3mm. Blue dye: food color (Americolor, USA).